Above-threshold multiphoton photoemission from noble metal surfaces

Marcel Reutzel, Andi Li, and Hrvoje Petek

Phys. Rev. B **101**, 075409 — Published 6 February 2020

DOI: 10.1103/PhysRevB.101.075409

Above-threshold multiphoton photoemission from noble metal surfaces

Marcel Reutzel,[1,2,‡] Andi Li[1], and Hrvoje Petek[1,‡]

[1]*Department of Physics and Astronomy and Pittsburgh Quantum Institute, University of Pittsburgh, Pittsburgh, Pennsylvania 15260, USA*

[2]*I. Physikalisches Institut, Georg-August-Universität Göttingen, Göttingen, Germany*

[‡]*email: marcel.reutzel@phys.uni-goettingen.de, petek@pitt.edu*

Abstract

Exciting solids with intense femtosecond laser pulses prompts electrons of the interrogated material to respond in highly non-linear manner, as is evident in the emission of high-order harmonic radiation and photoelectrons with kinetic energies well above that of the driving photons. Such high-field interactions can be resolved, for example, in above-threshold multiphoton photoemission (ATP) spectroscopy. In this work, we interrogate the nonlinear photoelectric responses of the pristine copper, silver, and gold noble metal surfaces in (111) and (100) crystal orientations in the perturbative regime. Using multi-photon photoemission spectroscopy (mPP) excited by finely tuned optical fields, we characterize enhancement of the mPP and ATP yields from (111) surfaces in selected $k_{||}$-momentum ranges when the occupied Shockley surface (SS) states are (near-)resonantly coupled by multi-photon transitions to image potential (IP) intermediate states in the excitation process. The ATP signal from the IP states of (111) surfaces is largely defined by their formation through polarization of SS electrons; this observation is contrasted with ATP experiments from the Ag(100) surface, for which the SS becomes an unoccupied resonance and the IP states can only be excited from bands with significantly more bulk character. In addition, based on the optical power and non-linear order dependent mPP spectra, we provide new evidence for ATP being a one-step, rather than a sequential process, as previously postulated.

I. INTRODUCTION

Above-threshold ionization (ATI) refers to processes where atoms and molecules absorb additional v photons above the minimum number of u that are necessary to overcome the ionization potential; photoelectrons with up to v quanta of excess kinetic energy are emitted creating replicas of the u-th order spectrum in an overall (u+v)-th order process [1,2]. When intense lasers excite solid-state materials, such highly nonlinear processes are termed above-threshold photoemission (ATP), in analogy to ATI. ATP can probe different phenomena in the strong and weak field regimes, as distinguished by the relative excitation field strength and quantified by the Keldysh parameter γ [3]. For $\gamma \ll 1$, in the nonperturbative regime, extreme optical phenomena like high-harmonic (HHG), and/or attosecond pulse generation occur [4,5]. With respect to ATP, strong-field photoemission has been observed from sharp metal tips [6-8], and plasmonic nanostructures [9-12]. By contrast, ATP from atomically flat surfaces typically occurs when excitation is performed in the perturbative regime ($\gamma \gg 1$). Several ATP studies reported multiphoton photoemission (mPP) excitation involving dipole transitions between the momentum-dispersive occupied and unoccupied surface states of noble metals [13-20]. Replica structures of the lowest order photoemission spectral feature detected in uPP have been detected in (u+v)PP (v=1,2,…), where each higher-order process appears with a substantially reduced photoemission yield.

We perform angle- ($k_{\|}$-momentum-) resolved high-order mPP spectroscopy to study ATP from crystalline copper, silver, and gold surfaces (m = 3-6). We record the multi-photon dynamics primarily within the *surface projected band gaps* of these metals, which support the partially occupied Shockley surface state (SS) [21,22], and the Rydberg-like series of image potential (IP) states or resonances [23,24]. The coupling of these quasi-two-dimensional states to atomic and

molecular adsorbates [25,26], as well as the electron dynamics of the pure [27,28] and adsorbate modified states [25,29] represent benchmarks for developing an understanding of light driven quantum state resolved electron dynamics of interest to metal quantum optics and surface photochemistry [20,28,30-35]; they are ideal models to study polaron formation in molecule covered surfaces [36-38], charge transfer dynamics at metal surfaces, and more complex interfaces [25,26,29,39-41], as well as the quantum control of electron dynamics [30,33,42-45]. Furthermore, their Rashba type spin-splitting [22,46-48], and topological nature [49] have aroused interest in contexts of spintronics and topological protection.

By exciting the IP←SS transition of (111) oriented noble metal surfaces (near-)resonantly with three IR-photons, we detect their lowest order 4PP and higher order ATP spectra. Our analysis of the photoemission order m and optical power dependent ATP spectra is consistent with a recent 2D Fourier transform (2D-FT) photoelectron spectroscopy study, which concluded that ATP of the occupied SS state is dominantly a one-step process of rectification of the coherent $(u+v)$-polarization [20]. This stands in contrast to the postulated two-step attribution of ATP, which has been adopted from ATI, where the above threshold process occurs by photoelectrons being generated first by absorbing u-photons and then absorbing another v-photons prior to emerging from the surface region [13-19]. Furthermore, we contrast our results for the (111) oriented surfaces with ATP spectra obtained from Ag(100), for which the Shockley state is predominantly unoccupied and resonant with bulk bands, where it can act as an intermediate state in excitation of the IP states.

II. EXPERIMENTAL MEHTODS

mPP spectroscopy on noble metal surfaces is performed in an ultrahigh vacuum chamber (UHV) with a base pressure of $<10^{-10}$ mbar. Single-crystal noble metal surface samples are prepared by cycles of Ar^+ ion sputtering and annealing [20 min sputtering: 1500 V, 3 μA; 10 min annealing: Ag(111), Au(111), Ag(100): 550 K; Cu(111): 800 K]; surface quality is judged by the work function energy, weak mPP signal at the secondary electron cutoff (work function edge) relative to the overall photoemission signal, as well as sharp spectroscopic peaks from the SS and IP states. All spectra are recorded at ambient temperature.

Wavelength tunable femtosecond laser pulses in a 930 - 550 nm (1.3 – 2.3 eV) range are generated with two noncollinear optical parametric amplifier (NOPA) lines, which are pumped at a 1 MHz pulse repetition rate by the second and third harmonics of a Clark MXR Impulse Yb doped fiber laser oscillator-amplifier system. Depending on wavelength, pulse durations are in the 20 – 30 fs range, as characterized by interferometric autocorrelation measurements [20,35]. Time broadening of the laser pulses by dispersion in the optical system is compensated by multiple reflections from negative dispersion mirrors.

mPP spectra are excited by passing *p*-polarized near-IR pulses through a 150 mm focusing lens into the UHV chamber at an angle of incidence of 45° with respect to the lens axis of a Specs Phoibos 100 hemispherical electron energy analyzer. An average power of 25-190 mW is focused onto the single crystal surfaces, to achieve a fluence of ≈0.3-2.5 mJ/cm^2 or an optical field strength of ≈10^9 V/m (estimated beam waist diameter on the surface is 100 μm); the electric field strengths on the surface is further controlled by translating the optical beam waist by moving the focusing lens

with respect to the sample surface while keeping the average power and pulse duration constant. Possible sample damage or signal distortion by space charge effects [50] do not occur based on the reproducibility of mPP spectra after irradiation of the same sample spot for several hours, and imperceptible effect of laser fluence on spectral broadening, respectively. The samples are aligned to detect normal emission or can be rotated in the optical plane to access a larger $k_{||}$-range. The photoelectron analyzer records the final state photoelectron energy-, E_f=E-E_F, *vs.* photoemission angle distribution with a 2D position sensitive electron counting detector. The angle is converted to $k_{||}$-momentum in $E_f(k_{||})$ photoelectron spectra, which we report.

III. Results and Discussion

The (111) and (100) surface band structures of noble metals have inverted projected band gaps centered at the $\bar{\Gamma}$-point ($k_{||}$ = 0 Å^{-1}), that extend from the lower, L_{sp}, to the upper, U_{sp}, bulk sp-bands (*cf.* band diagrams in Fig. 1). In the (111) orientation, the SS state of Cu, Ag, and Au surfaces, which exists because of the abrupt termination of the interatomic interactions, are occupied around their band minimum at the $\bar{\Gamma}$-point, and become unoccupied as they cross E_F at $k_{||}$≈0.1-0.2 Å^{-1} [21,22]; their band dispersion deviate modestly from quasi-free-electron like as they approach and hybridize with the bulk L_{sp}-band at $k_{||}$>0.2 Å^{-1} [51,52]. Moreover, these (111) surfaces each have an unoccupied Rydberg-like series of IP states labeled by an integer quantum number n that converges to the vacuum level as n increases [23]. The IP state wave functions reside mainly in the vacuum, but penetrate variously into the bulk [53], where they experience stronger electron-electron and electron-phonon interactions; therefore, the degree of their penetration substantially determines their

lifetimes [27,31,54]. For Cu(111) and Ag(111), the first n=1 IP state (IP1) lies in the band gap just below U_{sp}, and therefore penetrates into the bulk only evanescently, whereas the n≥2 IP states (IP2, IP3, …) become resonant with the U_{sp}-band. By contrast, for Au(111), the U_{sp}-band minimum is at a lower energy with respect to E_F causing the entire IP series to be resonant with it [53].

A. Cu(111)

We begin by examining the spectroscopy of (111) oriented surfaces by tuning the photon energy such that three-photons excite SS electrons (near-)resonantly with the IP state series, and additional one or more photons excites them further above the vacuum level, E_{vac}, in a m=4-6 photoemission process. The highly non-linear excitation scheme thereby enables effective detection of ATP involving well-defined occupied and unoccupied bands of noble metals in the perturbative regime.

Figure 1 shows $E_f(k_{||})$-resolved mPP spectra of the (111) oriented Cu, Ag, and Au surfaces; in the following, we discuss ATP of Cu(111) in detail, and subsequently compare the results to related mPP spectra obtained under similar conditions for the Ag(111) and Au(111) surfaces. In Fig. 1(a) (Cu(111), $\hbar\omega$ = 1.59 eV), the occupied part of the $SS^{(m)}$ state, as well as the $IP1^{(m)}$ and $IP2^{(m)}$ states, are shown for m = 4 and 5 photoexcitation processes. The detected $k_{||}$-range of the SS and the IP1 states is affected by the $k_{||}$-dependent crossing of SS above E_F, as well as the experimental analyzer acceptance angle. For Cu(111), the surface states dominate the mPP spectra particularly at $k_{||}$ where the signal is enhanced by resonant or near-resonant three-photon excitation of the IP←SS transition. The occupied SS below E_F can serve as the initial state for IP state excitation. Nevertheless, the unoccupied part of the SS state is also detected as an intermediate state, and its role in the mPP process will be discussed below. The binding energies and $k_{||}$-dispersions of the surface states are

consistent within the different orders of photoexcitation, as well as agree with published 1PP [22] and 2PP [24,55] spectra; minor deviations in the $k_{||}$-distributions are attributed to stray fields that affect detection of low kinetic energy photoelectrons.

We examine how resonant and near-resonant surface transitions in energy- and momentum-space affect the ATP yield. Figure 2 shows $E_f(k_{||})$-resolved mPP (ATP) spectra of Cu(111) excited with 1.53-eV, 1.57-eV, and 1.67-eV light pulses under otherwise comparable excitation conditions; m = 4-6 processes are observed. At $\hbar\omega$=1.53 eV [Fig. 2(a)], the three-photon IP1←SS transition is excited resonantly at $k_{||} \approx 0.0$ Å^{-1}. The different effective masses, and therefore $k_{||}$-dispersions, of the IP1 and SS bands cause the resonance condition to detune for $k_{||}>0.0$ Å^{-1}, where consequently photoemission yields decrease. When increasing the photon energy to $\hbar\omega$=1.57 eV, the IP1←SS transition is detuned from resonance over the entire $k_{||}$-range of the occupied SS state, but nevertheless the SS and IP band features are still detected in the 4PP and ATP spectra [Fig. 2(b)]. At $\hbar\omega$=1.67 eV, a three-photon resonant excitation occurs for the IP2←SS transitions at $k_{||} \approx 0.12$ Å^{-1}, but not at $k_{||} \approx 0.0$ Å^{-1} [Fig. 2(c)]. These resonance enhancements of three-photon absorption is replicated in ATP. In the subsequent sections, we will quantitatively evaluate the nonlinear excitations that contribute to these spectra based on the optical power and non-linear photoemission order m to provide further insights into the ATP mechanism.

First, however, in Fig. 3(a), we show an $E_f(k_{||})$-resolved mPP spectrum of Cu(111) for $0.0 \leq k_{||} \leq 0.45$ Å^{-1} when excited with $\hbar\omega = 1.66$ eV light pulses. As already described in Fig. 2(c), excitation of the IP2←SS transition proceeds resonantly by three-photon excitation at $k_{||} \approx 0.12$ Å^{-1}. Because the effective mass of SS$^{(4)}$ is less than that of the IP2$^{(4)}$ state, for $k_{||} > 0.15$ Å^{-1}, the resonant excitation becomes detuned, but nevertheless, the upwardly dispersing *unoccupied* part of the SS state is

detected (labelled $SS^{(5,unoc)}$). The probable photoemission pathway of $SS^{(5,unoc)}$ is indicated in the excitation diagram in Fig. 3(a): In a $k_{||}$-conserving process, the $SS^{(m,unoc)}$-state can only be populated by an one-photon transition from the bulk, *3D*-dispersive, L_{sp}-band, and subsequently be detected by four-photon excitation above the vacuum level in an overall fifth-order process (m = 5). In addition, we note that the unoccupied part of the SS state is sufficiently high in energy to be detected by further three-photon absorption, but its signal, labeled as $SS^{(4,unoc)}$, is at edge of the accessible $k_{||}$-range that is limited by the acceptance angle of the electron analyzer.

In the fifth-order process, however, $SS^{(5,unoc)}$ is detected and resolved in the 6.8 to 8 eV E_f-range for $0.2 < k_{||} < 0.43$ Å^{-1}; strikingly, its mPP yield is enhanced at $k_{||} \approx 0.43$ Å^{-1} where it is detected at the same $E_f(k_{||})$ as the $IP1^{(5)}$ photoemission spectral feature [vertical arrow in Fig. 3(a)]. Thus, for selected $k_{||}$, the overall 5PP process proceeds via an intermediate two-photon resonance between the unoccupied SS and IP1 states [excitation diagram in Fig. 3(a)]. Such complex ATP enhancement in $k_{||}$-space has been proposed in Ref. [18] for Ag(111); here, the presented 2D $E_f(k_{||})$-data clearly identify this resonance when compared to other $k_{||}$ where the $IP1^{(5)} \leftarrow SS^{(5,unoc)}$ transition is detuned. ATP enhanced by such high-order resonant transitions can thus facilitate the detection and analysis of photoemission spectral features at large $k_{||}$ that may be hidden below the photoemission horizon [56] in lower order multiphoton excitation.

Next, we consider how the IP states are excited if the IP1←SS transition is significantly detuned [Fig. 3(a)]. The IP1 state could be excited nonresonantly from SS by dephasing of the induced coherence, but the detuning of the IP1←SS transition by $\hbar\Delta \approx 0.6$ eV would require this to occur on <1 fs time scale for significant population to be transferred. Because the SS and IP1 state dephasing occurs on >20 fs time scales, however, such nonresonant excitation process cannot be effective

[43,57]. Instead, the IP1 state might also be excited from the L_{sp}-band. To evaluate which process might be dominant, we compare the mPP yields of the IP1 state in the occupied range of the SS state ($k_{||} \lesssim 0.2$ Å^{-1}), with those of $k_{||} \gtrsim 0.2$ Å^{-1}, where excitation cannot occur from SS without electrons improbably gaining $k_{||}$-momentum, and therefore energy, through scattering. The IP1 state yields vs. $k_{||}$ do not show a sharp falloff at $k_{||} \gtrsim 0.2$ Å^{-1}, while mPP intensity of the SS state drops abruptly by a factor ~50 when it transits above E_F [Fig. 3(a)]. Thus, the $k_{||}$-dependent signal from the IP1 state suggests that the portion of the IP1 state for $k_{||} \gtrsim 0.2$ Å^{-1} must either be excited from the L_{sp}-band, or starting from the occupied part of SS through some scattering process, which obscures its origin. Similar $k_{||}$-dependent mPP yield on Cu(111) was as well observed in Ref. [52], and is recorded in Fig. 3(b/c) for the Ag(111) and Au(111) surfaces. Thus, we speculate, that both the dephasing of the detuned IP1←SS excitation and the excitation from the bulk lead to the IP1 state population with the relative probability determined by the detuning, but our data does not allow us to separately quantify these photoexcitation pathways. We note that the $k_{||}$-dependent population of the IP states on metal surfaces is not necessarily only defined only by the excitation process, but may also be influenced by inter- and intraband energy and momentum scattering [58,59]. Yet, for Cu(111), interband scattering, for example, from the IP2 into the IP1 state can be neglected because IP2 is shorter lived than IP1 due to it stronger coupling to the bulk [60]. Furthermore, intraband scattering within the IP1 state is not expected to strongly affect its $k_{||}$-dependent populations within the excitation time scales.

B. Ag(111) and Au(111)

4PP and 5PP (ATP) spectra of Ag(111) and Au(111) surfaces show similar trends as described for Cu(111); in Fig. 1(b/c) and Fig. 3(b/c), $E_f(k_{||})$-spectra of these surfaces are plotted in a narrow and

a broader $k_{||}$-region, respectively, set by rotating the angle of the sample with respect to the electron analyzer. Both, the occupied and unoccupied parts of the SS state, are recorded. The photon energies are chosen such that the SS state has a two- or three-photon resonance with an IP state for a certain $k_{||}$; the non-resonant ATP from the SS state has been described for both surfaces in Ref. [18-20]. As for Cu(111), ATP yield enhancement can be observed in (near-)resonant excitation of the surface states, independent of whether the SS state acts as the occupied initial state [Fig. 1(b/c)] or as an unoccupied intermediate state in the multi-photon process [Fig. 3(b/c)]. Furthermore, in Fig. 3, we have chosen the photon energies such that lowest order photoemission occurs for u = 4, 3, and 5 for Cu(111), Ag(111) and Au(111), respectively. In each case, the expected binding energies, effective masses, and mPP (ATP) yield enhancement in resonant coupling of the surface states are observed, implying thus similar photoexcitation pathways, irrespective on the minimum number of photons u necessary to overcome the work function. mPP spectra of Ag(111) show, in addition to the surface states, the coherent resonant four-photon transition between the bulk sp-bands, labelled $sp^{(m)}$ in Fig. 1(b) [55]. We note, that for all studied surfaces the large bandwidth of the ultrafast excitation pulses prevents resolution of the Rashba spin-splitting of the surface states [22,46-49].

While similar surface state signal as for Cu(111) and Ag(111) is observed in mPP spectra of Au(111) (Fig. 1), its ratio of signal-to-the-featureless-background is considerably worse. This can be attributed to the fact that the entire IP state series of Au(111) is resonant with the U_{sp}-band, while for Ag(111) and Cu(111), the IP1 state is not. The IP1 state propagation and damping in the bulk of Au(111), can therefore redistribute the surface electrons to the bulk, as well as increase their bandwidths, both of which could contribute to the structureless spectrum that overlaps with the IP states.

Finally, we emphasize that highly nonlinear SS state excitation occurs for all three (111) oriented noble metal surfaces when exciting with IR frequencies. Thus, these nonlinear responses appear to be a general characteristic of metals that does not strongly depend on the precise structure of their electronic bands, dielectric functions, or their many-particle screening (plasmonic) responses.

C. Ag(100)

So far, our data and analysis concerned the energy- and $k_{||}$-momentum resolved ATP spectra of the (111) oriented noble metal surfaces, where the (near-)resonant coupling of the IP←SS transition dominates the mPP spectra. Next, we extend our study to the (100) facet of the Ag crystal (Fig. 4), which involves a qualitatively different occupied and unoccupied surface projected band structure. The relevant differences between the band structures of the two high-symmetry crystal orientations is evident by comparing Figs. 1(b) and 4(c): Whereas E_F at the $\bar{\Gamma}$-point of the Ag(111) surface lies in the surface projected band-gap, for Ag(100), the L_{sp}-band extends to the $X_{4'}$ point roughly 1.6 eV above E_F [53,61]. Because the band gap of the Ag(100) surface occurs in a different energy range, the same physics that gives rise to SS on the (111) surfaces leads to a predominantly unoccupied Shockley surface resonance (SR) on Ag(100), which is centered 1.3 eV above E_F [53,61]. Because SR and the resonant L_{sp}-band form a hybridized density of states (DOS), SR acquires a large width, implying a fast surface-to-bulk delocalization. The broad DOS of SR extends even to below E_F, where it is partially occupied. The intermediate IP states, however, lie in the surface projected band-gap, where their penetration into the bulk is weak [24,53].

Figure 4(a) shows an $E_f(k_{||})$-resolved mPP (ATP) spectra of Ag(100) excited with $\hbar\omega$=1.71 eV photons. Whereas the mPP spectra of Ag(111) for IR excitation show high peak-to-background ratios

with spectrally narrow mPP features, for Ag(100), spectrally broad features are observed, which we attribute to SR. According to Fig. 4(a), the SR has a broad linewidth in the 1-2 eV range, reflecting its resonant coupling with the L_{sp} band that suggests that in-fact the surface-to-bulk transfer occurs on a sub-femtosecond time scale. Because partial DOS of SR below E_F is occupied, SR can act either as the initial or intermediate state in the mPP process, but is unlikely to serve as both, because that would involve intraband absorption. We note, that $SR^{(4)}$ (ATP) is substantially broader than $SR^{(3)}$, which might reflect the different contributions from the occupied and the unoccupied part of SR. In addition, a sharp, but relatively weak $IP1^{(4)}$ state is detected; the Fermi edge, $E_F^{(m)}$, is resolved both in 3PP and 4PP.

In high-order IR light excitation, the surface projected band structure around E_F significantly impacts the photoexcitation of the IP states. On Ag(111), well-defined spectroscopic features of the IP1 and IP2 states are detected in ATP. The IP states can be excited either from SS or L_{sp}-bands, whereas the (near-)resonant coupling of the IP←SS transition dominates the mPP yield. On Ag(100), however, the IP states must be excited either from the occupied part of the SR or from the L_{sp}-band; for both scenarios substantial bulk character of the initial state is expected. For IR excitation [1.71-eV in Fig. 4(a)], a three-photon coupling of the occupied part of SR into the IP1 state is largely detuned, which makes such an excitation pathway less probable. Instead, we assume the initial excitation of L_{sp}-electrons via intermediate polarization of the energetically broad unoccupied part of the SR to populate the IP1 state. Thus, there is no pure surface photoexcitation pathway through which the IP states can be detected, as in the case on Ag(111); therefore, the IP1 peak is relatively weak compared with the SR features. This stands in contrast to excitation of Ag(100) with $\hbar\omega$=2.12 eV photons [Fig. 4(b)]. Here, the IP1 state is by far the dominant feature in the 3PP and ATP spectra,

as, most likely, in this case, the IP1 state can be near-resonantly excited by two-photon absorption from the occupied part of SR. Thus, for both Ag(111) and (100) surfaces, the (near-)resonant excitation from SS and SR appears to promote mPP and ATP via the IP1 state.

D. Perturbative ATP

Because ATP has a higher nonlinearity than the primary mPP signal of the lowest order *u*, it is insightful to characterize the effect of the optical fluence on the ATP yield. Therefore, in Fig. 5, we show E_f-resolved ATP spectra of Cu(111) for excitation with increasing laser power ($k_{||}$ = 0.0 Å^{-1}); photoemission yields of the IP1 and SS states increase for both the resonant [Fig. 5(a), $\hbar\omega$ = 1.56 eV, Res], as well as the detuned [Fig. 5(b), $\hbar\omega$ = 1.64 eV, IP1&SS] excitation. A quantitative evaluation of the peak signal amplitudes is given in the insets: On the double-logarithmic scale, the mPP yield scales *linearly* with increasing laser power (proxy for the laser fluence); the data fit well to the power scaling law ~I^k, where *k* approximates the photoemission order *m* of the primary signal and its ATP replicas (*i.e.* $k \approx m$; the fitted values are given in the insets of Fig. 5). Therefore, independent on whether photoemission occurs in the lowest order (m=u=4) or in ATP (m=u+v), the photoemission yield scales with the overall non-linear photoemission order *m*. At the highest fluences, the 4PP process appears to be leveling off, which is expected if ATP increases with a higher power scaling law at the cost of reducing the signal from the lower orders [Fig. 5(a)]. Moreover, E_f of the photoemission spectral features is *constant* with the increasing optical fluence [Fig. 5(c)].

Further insight into the ATP process becomes accessible when quantifying the E_f-energy and the mPP yield of the surface states for increasing non-linear order *m* at otherwise constant excitation conditions. We evaluate mPP spectra, such as shown in Fig. 2, by plotting the nonlinear photoemission order *m* dependent E_f-values and the peak amplitudes of the surface states of Cu(111)

for both the resonant ($\hbar\omega$ = 1.53 eV, $k_{||}$ = 0.0 Å^{-1}, Res) and detuned ($\hbar\omega$ = 1.67 eV, $k_{||}$ = 0.0 Å^{-1}, IP1&SS) excitation in Fig. 6.

The E_f-energies of the photoemission spectral features increase linearly with the photoemission order m [Fig. 6(a)], whereas the slopes approximately scale with the used photon energy $\hbar\omega$, regardless of the resonance condition. This is expected in a perturbative process because the photoelectron energy is determined by absorption of m quanta of light. A deviation from this relationship might occur if the applied field dresses the electronic band structure of the sample or if the optical field modifies the vacuum level causing field emission [6,62,63].

The measurements in Figs. 5 and 6 show that the reported ATP processes occur in the perturbative regime where these high-order photoemission yields build up by the optical field exciting dipole transitions within $\boldsymbol{k}$-dispersive electronic bands of the noble metal surfaces with substantially diminished probabilities as m increases. In other high-optical field excitation experiments on solid state materials, such as in laser power dependent electron emission from sharp metal tips, it was shown that both the electron yield [6,7] and kinetic energy of the yield maximum [6] can deviate from expectations for a perturbative process due to nonperturbative contributions from field emission processes. Based on the distinctly exponential laser power dependent yields in Fig. 5, we conclude that our reported ATP signal from flat noble metal surfaces occurs within the perturbative regime and thus dominantly occurs by coherent dipole transitions excited within the $\boldsymbol{k}$-dispersive electronic band structure. This is in accordance with a Keldysh parameter [3,8], which we estimate for the highest laser power in Fig. 5 to be $\gamma \approx 13$.

E. One vs. two Step ATP

In resonant, as well as in detuned excitation, mPP yields from the surface states drop approximately with an exponential dependence on the photoemission order m [Fig. 6(b)]. Significantly, in the detuned excitation, where the SS and IP1 signals are resolved separately, we find that the IP1 state intensity decreases faster with m than that of the SS state. For example, in Fig. 2, the mPP signal of the SS state becomes dominant over the IP1 state signal for $m \geq 5$. Consequently, for $m = 6$, the $SS^{(6)}$ feature is still detected, while the $IP1^{(6)}$ feature does not appear above the noise level. This trend for more effective ATP of the SS over the IP1 state is observed in the entire studied optical excitation power range [Fig. 5(b)], as well as is consistent with an earlier nonresonant study of mPP study from Ag(111) [20], and the ATP data obtained for Au(111) [Fig. 1(c) and 3(c)].

Being thus observed for three surfaces of (111) orientation surfaces in a broad excitation frequency and power range, we conclude that the nonresonant ATP of the SS state is more probable compared to an excitation via the IP intermediate states, independent on the specific electronic band structure of the studied metal, and related differences in the relative lifetimes of the virtual and real (IP1) intermediate states at the three-photon energy. Instead, the differing ATP yields of the surface states seem to be a more general phenomenon related to the remarkably non-linear m-photon response of SS electrons on noble metal surfaces. Hence, we examine the differences between the coherent one-step nonresonant mPP (ATP) of the initially occupied SS state, with a two-step process that occurs through multiphoton population of the intermediate IP states.

Although ATP has been observed on several metal surfaces [13-20], the process by which an electron absorbs multiple photon quanta before emerging into vacuum has in most cases so far not been discussed based on experiments that are capable of assessing how it occurs. The conventional view in the literature, probably adopted from atomic ATI [2], has been that ATP occurs as a sequential process: electrons excited above the vacuum level in lowest possible order u absorb additional v photons before leaving the surface region where momentum for inducing optical transitions can be supplied [13-19]. The mPP and ATP process of SS electrons on Au(111) surface upon 1.55 eV photon excitation was measured by Sirotti *et al.* [19]. They modeled it as a resonant process, where they assumed that the $22\times\sqrt{3}$ surface reconstruction causes band folding in the band gap to generate resonant excitations, though if such resonances did exist, there is no spectroscopic evidence for them. Instead we show that the nonlinear excitation of SS occurs on the other unreconstructed noble metal surfaces, and therefore is a nonlinear property of metals that requires further theoretical elaboration. Moreover, recently, we obtained evidence that ATP from the SS state of Ag(111) is a one-step process [20] like linear photoemission [64]: When an intense optical field interacts with electrons in the SS state of Ag(111), they respond by oscillating coherently at multiple harmonics of the driving field with a progressively decreasing amplitude, which can potentially result in ATP. Thus, both mPP and ATP can be generated by rectification of high-order nonlinear polarization fields to produce photoelectron currents at the final state energies of the lowest order u as well as all higher orders $u+v$. Following the arguments of Ref. [20], the one-step $m=u+v$-photon ATP process of SS state is more likely than the same order process via the excitation of the IP intermediate state. In a two-step excitation process, upon photoexcitation of electron-hole pairs from the SS state to form a transient excitonic precursor, the IP state first has to form through screening of

the Coulomb interaction on the subfemtosecond time scales [35,65], before it can be photoemitted in the same non-linear order as the SS state. Thus, even though the SS and IP state photoelectrons are generated in the same overall photoemission order m, their photoexcitation processes are qualitatively different, and therefore affect their photoemission yields.

While the competition between such high-order coherent process can explain the reversed intensity ratio of the SS and IP1 state in ATP, we would not expect it to be affected in a sequential ATP process: For the (111) oriented noble metal surfaces under consideration, the final photoelectron states are indistinguishable, independent on whether they are excited from the SS or a transiently populated IP1 state. Thus, the subsequent excitation of these above-vacuum states in the process of electron escape would not differentiate between electrons that have occupied the SS or IP bands. Consequently, from a two-step sequential process, we would expect replicated, rather than inverted intensity ratios. Nevertheless, a fuller understanding of ATP requires more rigorous modeling, for example, based on response theory [66], which, however, is beyond the scope of this work.

Finally, we would like to adumbrate that ATP, as identified by the replicated photoemission spectral features in the one-color mPP experiment, may be described in a Floquet picture [67]. The time periodic driving field can perturb the band structure to induce a manifold of Floquet replicas of the Bloch bands separated by $\pm N\hbar\omega$; the photoemission experiment then detects these bands for $+N \geq u$ as mPP or ATP if they lie above the vacuum level, but $+N < u$ bands remain undetected (N is an integer). Floquet bands have previously been reported in topological insulators using two-color IR-UV angle-resolved photoelectron spectroscopy, which could detect the ladder of Floquet states that are excited below the vacuum level [68]; further experimental scrutiny of the Floquet physics is desirable in both, the one- and the two-color photoemission experiments.

IV. Conclusions & Outlook

In conclusion, we have investigated $E_f(k_{||})$-resolved ATP from a material and a crystal orientation perspective with tunable photon energies. A detailed overview of the (111)- and (100)-oriented copper, silver, and gold surfaces shows that ATP is a general phenomenon in intense laser excitation of metal surfaces through a perturbative mPP process. Employing driving frequencies in the IR for highly non-linear excitation ($m \geq 3$), mPP (ATP) can be enhanced by coupling distinct resonance conditions between the SS state of (111) surfaces and the series of IP states. We find that the SS state has a dominant role in the IP state excitation and highlight that its unoccupied range above E_F becomes accessible in high-order mPP experiments. In addition, we provide further evidence that ATP from the occupied SS state occurs through a one-step process.

Besides enhancement by the resonant coupling of single-particle transitions, we expect that ATP, as a highly non-linear process, could be strongly dependent on the dielectric response and the plasmonic properties of the studied material. For example, for epsilon-near-zero (ENZ) materials, it was shown that the optical response is dominantly nonlinear and nonperturbative [69], leading to a strong enhancement of HHG [70]; for Ag(111), the ENZ condition strongly affects optical second-harmonic generation [71] and 2PP yield in the UV spectral region [55]. We expect ATP driven at photon energies close to ENZ to be highly effective and to enable the study non-perturbative physics from well-defined surfaces at moderate laser powers, with the full capabilities of time- and angle-resolved multiphoton photoelectron spectroscopy.

Finally, we propose ATP as an alternative method to access coherent electron dynamics at large $k_{||}$. The experimentally accessible $k_{||}$-range of angle-resolved photoemission experiments is limited by the identity $k_{||} = \sqrt{2m_e E_{kin}/\hbar^2}\sin(\vartheta)$ (m_e: electron mass, ϑ: photoemission angle); excitation

with optical frequencies in the mPP experiment leads to small kinetic energies (E_{kin}). As E_{kin} of the photoemission spectral features in the ATP experiment scales linearly with the photoemission order, $E_{kin} \sim m\hbar\omega$ [Fig. 6(a)], higher $k_{||}$, and thus deeper regions in the Brillouin zone become accessible. ATP might thus be considered as a complementary photoelectron spectroscopy approach to experiments using XUV sources to gain access to the electron dynamics at large $k_{||}$, *e.g.* Ref. [72-74]. We emphasize, that when only employing optical frequencies in the experiment, all time-resolved methods developed for this frequency range are available and could thus be applied to probe characteristic points throughout the Brillouin zone.

Acknowledgements

We thank Branko Gumhalter for fruitful discussions. The authors gratefully acknowledge financial support from DOE-BES Division of Chemical Sciences, Geosciences, and Biosciences Grant No. DE-SC0002313. M. R. acknowledges support through the Feodor Lynen Fellowship Program from the Alexander von Humboldt Foundation.

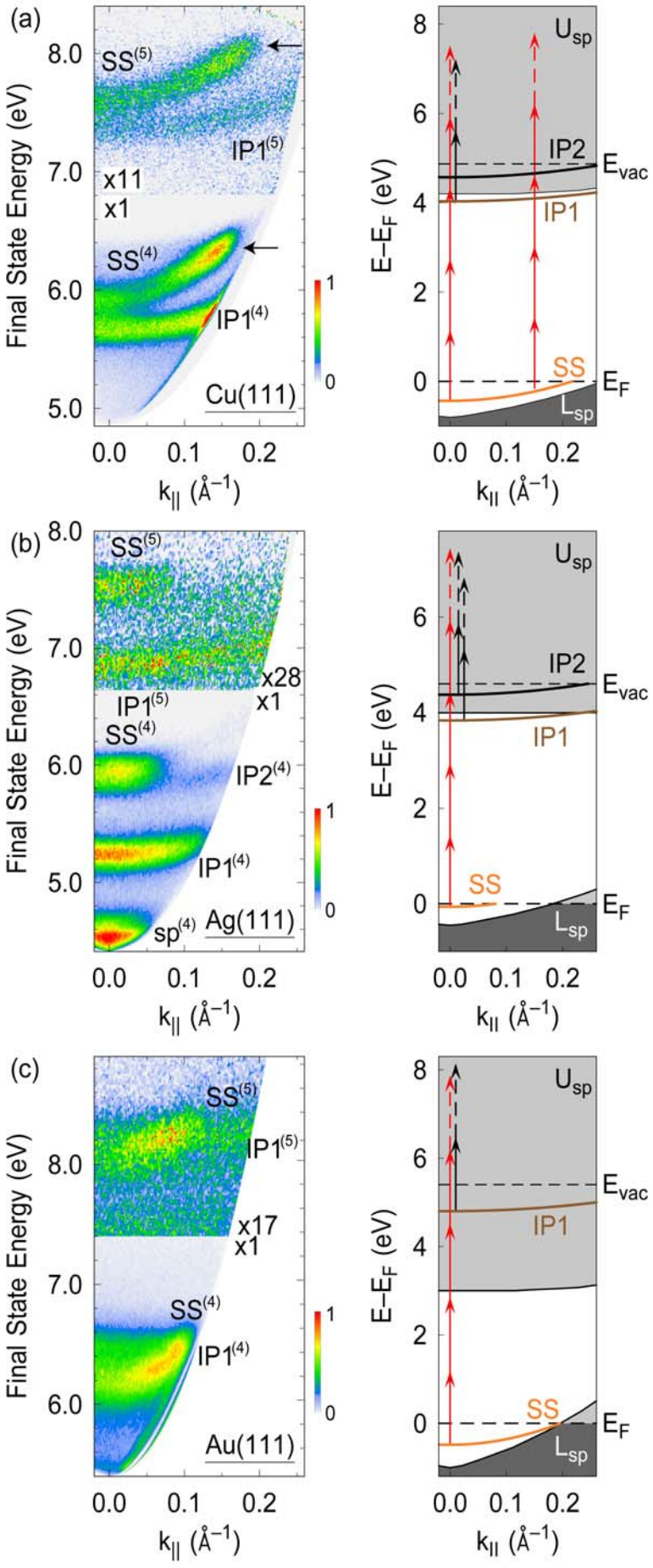
(a)
Final State Energy (eV)
8.0
7.0
6.0
5.0
SS(5)
IP1(5)
x11
x1
SS(4)
IP1(4)
Cu(111)
1
0
0.0
0.1
0.2
k|| (Å−1)
E–EF (eV)
8
6
4
2
0
Usp
IP2
Evac
IP1
SS
EF
Lsp
(b)
SS(5)
x28
x1
IP1(5)
SS(4)
IP2(4)
IP1(4)
sp(4)
Ag(111)
(c)
SS(5)
IP1(5)
x17
x1
SS(4)
IP1(4)
Au(111)

Figure 1| $E_f(k_{||})$-resolved mPP (ATP) spectra of (a) Cu(111), (b) Ag(111), and (c) Au(111) surfaces excited with $\hbar\omega$=1.59 eV, 1.50 eV and 1.67 eV photons, respectively; photoemission spectral features are labelled and the dominant excitation pathways are indicated in the surface projected band structures. mPP (ATP) yield (color-coded) is detected from the $IP1^{(m)}$, and $SS^{(m)}$ states for m = 4, 5. In addition, the $IP2^{(m)}$ state is resolved on Cu(111) (horizontal arrow) and Ag(111), where mPP yield is enhanced due to (near-)resonant excitation from the SS state at $k_{||}\approx0.12$ Å^{-1} and $k_{||}\approx0.00$ Å^{-1}, respectively. On Ag(111), in addition, the direct bulk sp-band transition, $sp^{(4)}$, is observed. In the excitation diagram, 4PP of the SS state and the IP states is indicated by red and black arrows, respectively; ATP is indicated by dashed arrows.

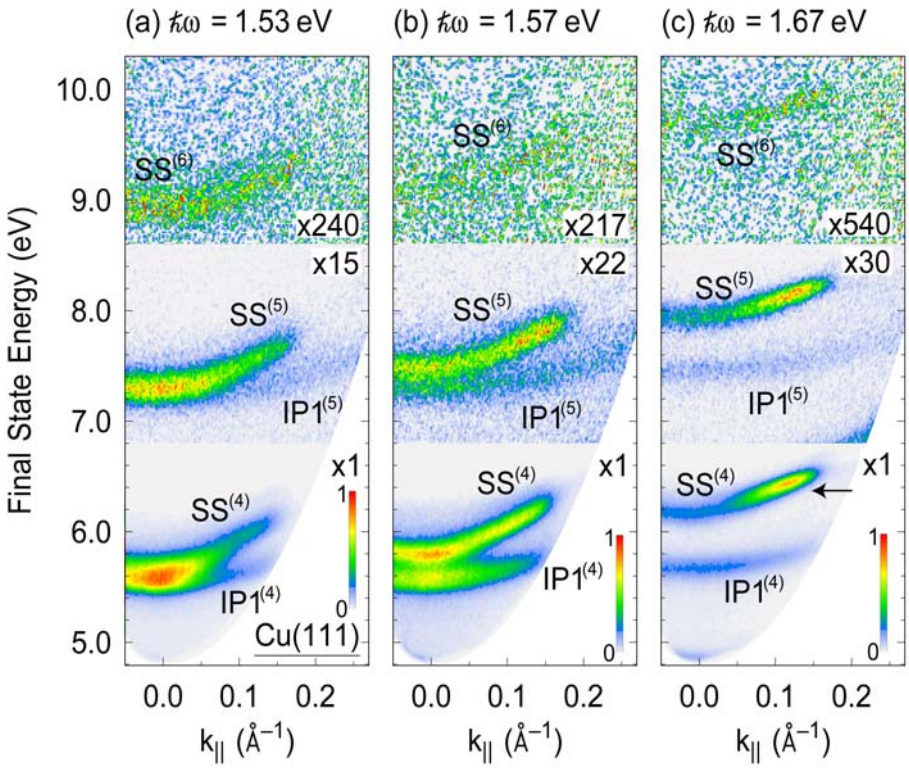

Figure 2| Photon energy dependent mPP (ATP) spectroscopy of Cu(111) in photoemission order m = 4 – 6 taken with the same average laser power; the color legends are scaled separately for each $\hbar\omega$. $E_f(k_{||})$-resolved mPP spectra are excited with (a) $\hbar\omega$=1.53, (b) $\hbar\omega$=1.57, and (c) $\hbar\omega$=1.67 eV light. The photon energies are chosen such, that three-photon excitation from the SS state is (a) resonant with the IP1 state at $k_{||} \approx 0$ Å^{-1}; (b) is detuned from resonance in the entire $k_{||}$-range; and (c) becomes resonant with the IP2 state at $k_{||} \approx 0.12$ Å^{-1} (horizontal arrow).

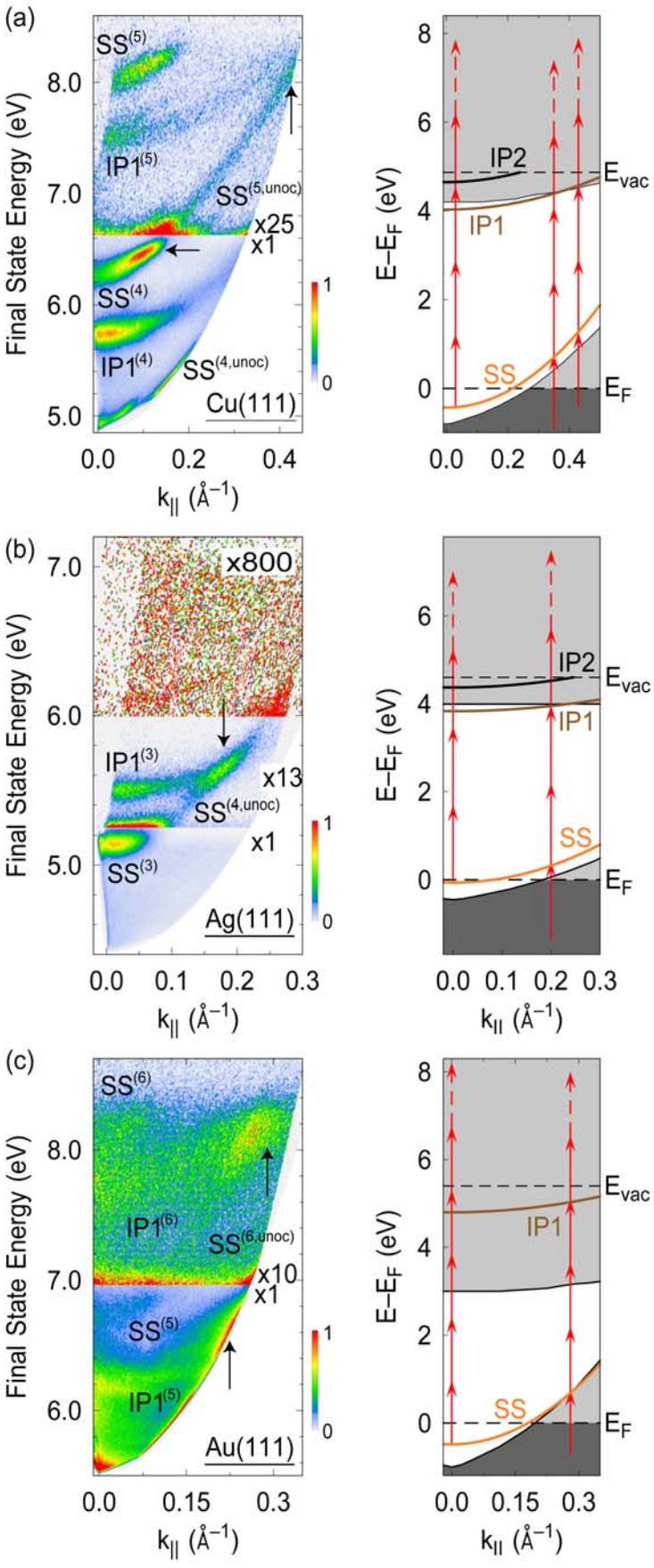
(a)
SS(5)
IP1(5)
SS(5,unoc)
x25
x1
SS(4)
IP1(4)
SS(4,unoc)
Cu(111)
Final State Energy (eV)
k|| (Å−1)
E–EF (eV)
IP2
IP1
SS
Evac
EF
(b)
x800
IP1(3)
x13
SS(4,unoc)
x1
SS(3)
Ag(111)
(c)
SS(6)
IP1(6)
SS(6,unoc)
x10
x1
SS(5)
IP1(5)
Au(111)

Figure 3| $E_f(k_{||})$-resolved mPP (ATP) spectra for large $k_{||}$ of (a) Cu(111), (b) Ag(111), and (c) Au(111) excited with $\hbar\omega$=1.66, 1.77, and 1.38 eV light; $\hbar\omega$ is chosen such that lowest order photoemission u overcomes the work function in 4-, 3-, and 5-photon processes, respectively. The surface projected band structures show dominant excitation pathways coupling the IP1←SS transition at large $k_{||}$. (a) The IP2←SS transition is excited resonantly for $k_{||} \approx 0.12$ Å^{-1} (horizontal black arrow). For $k_{||} \gtrsim 0.2$ Å^{-1}, the parabolically dispersing SS state crosses E_F and becomes unoccupied; its unoccupied portion is excited from the bulk sp-band and detected as an intermediate state in 4PP and 5PP processes. For $k_{||} \approx 0.45$ Å^{-1}, the IP1 state is excited resonantly via the unoccupied SS state in an intermediate two-photon resonance (vertical black arrow). (b)/(c) Similar to Cu(111), mPP enhancement is observed for Ag(111) and Au(111) at large $k_{||}$, where the IP1←SS transition proceeds resonantly (vertical arrows). The Ag(111) spectra for u = 3 do not record a distinct ATP feature at the used excitation fluence.

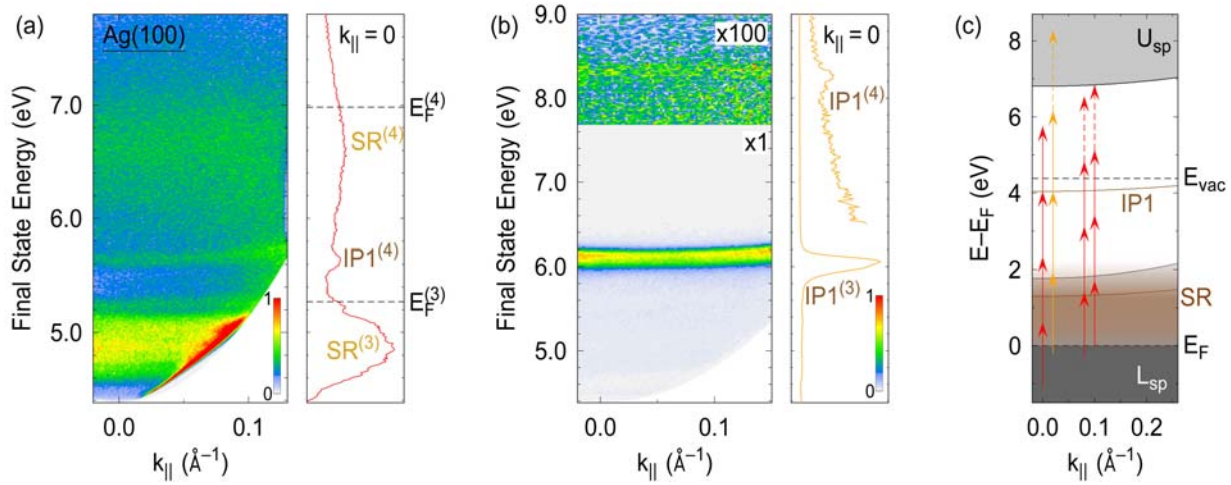

Figure 4| $E_f(k_{||})$-resolved mPP (ATP) spectra of Ag(100) excited with (a) $\hbar\omega$=1.71 and (b) $\hbar\omega$=2.12 eV light; photoemission spectral features are labelled in the energy-profiles taken for $k_{||}$ = 0.0 Å^{-1}. (a) In IR excitation, the IP1 state is only detected in 4PP; E_F and SR are detected in 3PP and 4PP (ATP). (b) For $\hbar\omega$=2.12 eV, the IP1 state is detected in 3PP and 4PP (ATP). (c) $k_{||}$-resolved excitation diagram for $\hbar\omega$=1.71 (red) and $\hbar\omega$=2.12 eV (orange) light. The IP1 state is located in the surface projected band-gap (white region) between the L_{sp} and U_{sp}. The spectrally broad SR (brown) is resonant with the L_{sp}-band and extends below E_F.

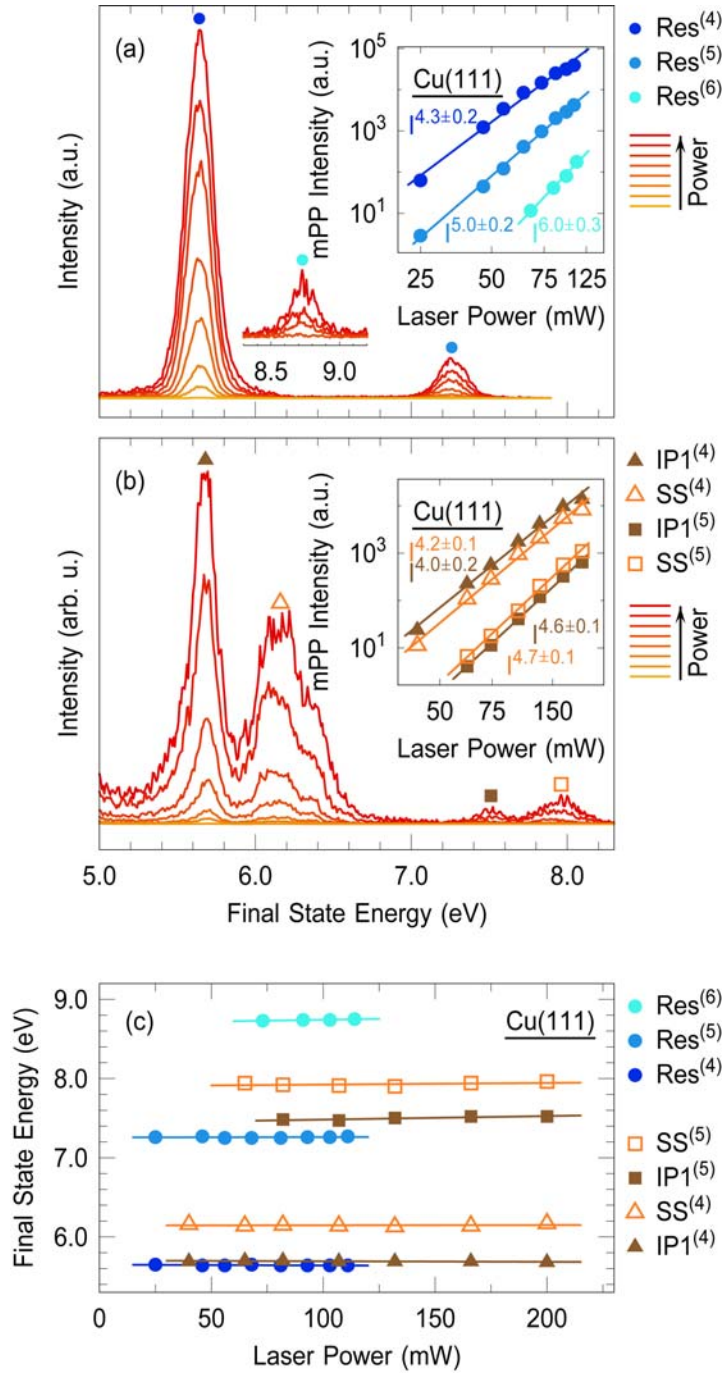

Figure 5| Power-dependent mPP (ATP) spectra of Cu(111) excited with (a) $\hbar\omega$=1.56 eV (resonant, Res$^{(m)}$) and (b) $\hbar\omega$=1.64 eV (detuned, IP1$^{(m)}$&SS$^{(m)}$) light at $k_{||}$ = 0.0 Å^{-1}; 6PP data is shown in the left inset of (a). In the insets, the mPP intensities are plotted as a function of the average laser power using a double-logarithmic scale for m = 4-6. The data are fitted with a power law scaling, I^k, where k approximates the photoemission order m, i.e. $k \approx m$; fitted values of k, including the standard error, are given in the inset. (c) The laser power dependent peak energies for resonant and detuned excitation of the IP1←SS transition.

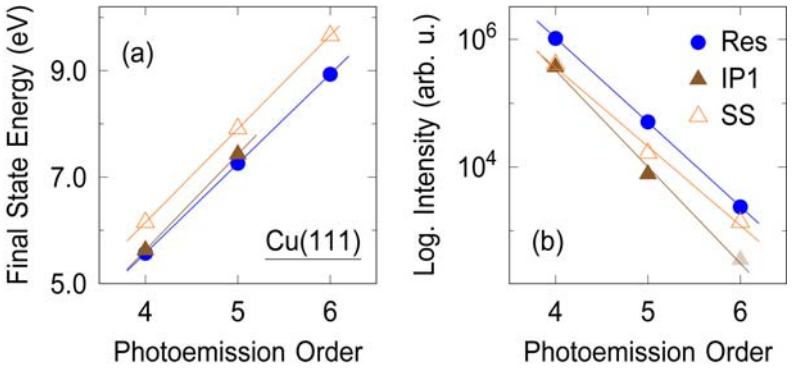

Figure 6| Quantitative evaluation of mPP (ATP) spectra of Cu(111) shown in Fig. 2 ($k_{||} \approx 0.0$ Å^{-1}). The data are obtained from the resonant (Res) and detuned (IP1&SS) excitation with $\hbar\omega$=1.53 eV and $\hbar\omega$=1.67 eV light, respectively. (a) The final state energy of the surface states shifts linearly with the photoemission order m. (b) The intensity of the surface states decreases exponentially with photoemission order m, but the IP1 state intensity drops faster than that of the SS state. The IP1 state intensity for m = 6 is indicated as a shaded brown triangle because it is within the noise level.

[1] P. Agostini, F. Fabre, G. Mainfray, G. Petite, and N. K. Rahman, Phys. Rev. Lett. **42**, 1127 (1979).

[2] W. Becker, F. Grasbon, R. Kopold, D. B. Milošević, G. G. Paulus, and H. Walther, in *Advances In Atomic, Molecular, and Optical Physics*, edited by B. Bederson, and H. Walther (Academic Press, 2002), pp. 35.

[3] L. V. Keldysh, Sov. Phys. JETP **20**, 1307 (1965).

[4] F. Krausz and M. Ivanov, Rev. Mod. Phys. **81**, 163 (2009).

[5] S. Ghimire and D. A. Reis, Nat. Phys. **15**, 10 (2019).

[6] M. Schenk, M. Kruger, and P. Hommelhoff, Phys. Rev. Lett. **105**, 257601 (2010).

[7] R. Bormann, M. Gulde, A. Weismann, S. V. Yalunin, and C. Ropers, Phys. Rev. Lett. **105**, 147601 (2010).

[8] M. Krüger, M. Schenk, M. Förster, and P. Hommelhoff, J. Phys. B. **45**, 074006 (2012).

[9] M. Merschdorf, W. Pfeiffer, A. Thon, S. Voll, and G. Gerber, Appl. Phys. A **71**, 547 (2000).

[10] P. Dombi, A. Hörl, P. Rácz, I. Márton, A. Trügler, J. R. Krenn, and U. Hohenester, Nano Lett. **13**, 674 (2013).

[11] M. Dąbrowski, Y. Dai, and H. Petek, J. Phys. Chem. Lett. **8**, 4446 (2017).

[12] M. Sivis, N. Pazos-Perez, R. Yu, R. Alvarez-Puebla, F. J. García de Abajo, and C. Ropers, Communications Physics **1**, 13 (2018).

[13] W. S. Fann, R. Storz, and J. Bokor, Phys. Rev. B **44**, 10980 (1991).

[14] M. Aeschlimann, C. A. Schmuttenmaer, H. E. Elsayed-Ali, R. J. D. Miller, J. Cao, Y. Gao, and D. A. Mantell, J. Chem. Phys. **102**, 8606 (1995).

[15] F. Banfi, C. Giannetti, G. Ferrini, G. Galimberti, S. Pagliara, D. Fausti, and F. Parmigiani, Phys. Rev. Lett. **94**, 037601 (2005).

[16] F. Bisio, M. Nývlt, J. Franta, H. Petek, and J. Kirschner, Phys. Rev. Lett. **96**, 087601 (2006).

[17] G. Saathoff, L. Miaja-Avila, M. Aeschlimann, M. M. Murnane, and H. C. Kapteyn, Phys. Rev. A **77**, 022903 (2008).

[18] F. Bisio, A. Winkelmann, C.-T. Chiang, H. Petek, and J. Kirschner, J. Phys.: Condens. Matter **23**, 485002 (2011).

[19] F. Sirotti, N. Beaulieu, A. Bendounan, M. G. Silly, C. Chauvet, G. Malinowski, G. Fratesi, V. Véniard, and G. Onida, Phys. Rev. B **90**, 035401 (2014).

[20] M. Reutzel, A. Li, and H. Petek, Physical Review X **9**, 011044 (2019).

[21] W. Shockley, Physical Review **56**, 317 (1939).

[22] F. Reinert, G. Nicolay, S. Schmidt, D. Ehm, and S. Hüfner, Phys. Rev. B **63**, 115415 (2001).

[23] P. M. Echenique and J. B. Pendry, J. Phys. C **11**, 2065 (1978).

[24] W. Steinmann, Appl. Phys. A **49**, 365 (1989).

[25] X. Y. Zhu, Surf. Sci. Rep. **56**, 1 (2004).

[26] J. P. Gauyacq, A. G. Borisov, and M. Bauer, Prog. Surf. Sci. **82**, 244 (2007).

[27] P. M. Echenique, R. Berndt, E. V. Chulkov, T. Fauster, G. A., and U. Höfer, Surf. Sci. Rep. **52**, 219 (2004).

[28] T. Fauster, M. Weinelt, and U. Hofer, Prog. Surf. Sci. **82**, 224 (2007).

[29] J. Güdde, W. Berthold, and U. Höfer, Chem. Rev. **106**, 4261 (2006).

[30] U. Höfer, I. L. Shumay, C. Reuss, U. Thomann, W. Wallauer, and T. Fauster, Science **277**, 1480 (1997).

[31] P. M. Echenique, J. M. Pitarke, E. V. Chulkov, and A. Rubio, Chem. Phys. **251**, 1 (2000).

[32] H. Petek, M. J. Weida, H. Nagano, and S. Ogawa, Science **288**, 1402 (2000).

[33] J. Güdde, M. Rohleder, T. Meier, S. W. Koch, and U. Höfer, Science **318**, 1287 (2007).

[34] R. D. Muiño, D. Sánchez-Portal, V. M. Silkin, E. V. Chulkov, and P. M. Echenique, Proc. Nat. Acad. Sci. **108**, 971 (2011).

[35] X. Cui, C. Wang, A. Argondizzo, S. Garrett-Roe, B. Gumhalter, and H. Petek, Nat. Phys. **10**, 505 (2014).

[36] N.-H. Ge, C. M. Wong, R. L. Lingle, J. D. McNeill, K. J. Gaffney, and C. B. Harris, Science **279**, 202 (1998).

[37] P. Szymanski, S. Garrett-Roe, and C. B. Harris, Prog. Surf. Sci. **78**, 1 (2005).
[38] J. Stähler, U. Bovensiepen, M. Meyer, and M. Wolf, Chem. Soc. Rev. **37**, 2180 (2008).
[39] C. D. Lindstrom, M. Muntwiler, and X. Y. Zhu, The Journal of Physical Chemistry B **109**, 21492 (2005).
[40] S. Mathias *et al.*, Phys. Rev. Lett. **104**, 066802 (2010).
[41] M. Shibuta, N. Hirata, R. Matsui, T. Eguchi, and A. Nakajima, J. Phys. Chem. Lett. **3**, 981 (2012).
[42] H. Petek, A. P. Heberle, W. Nessler, H. Nagano, S. Kubota, S. Matsunami, N. Moriya, and S. Ogawa, Phys. Rev. Lett. **79**, 4649 (1997).
[43] S. Ogawa, H. Nagano, H. Petek, and A. P. Heberle, Phys. Rev. Lett. **78**, 1339 (1997).
[44] H. Petek and S. Ogawa, Annu. Rev. Phys. Chem. **53**, 507 (2002).
[45] M. Aeschlimann *et al.*, Science **333**, 1723 (2011).
[46] K. Yaji, A. Harasawa, K. Kuroda, R. Li, B. Yan, F. Komori, and S. Shin, Phys. Rev. B **98**, 041404 (2018).
[47] R. Arafune, N. Takagi, and H. Ishida, Prog. Surf. Sci. **93**, 177 (2018).
[48] J. H. Dil, F. Meier, and J. Osterwalder, J. Electron. Spectrosc. Relat. Phenom. **201**, 42 (2015).
[49] B. Yan *et al.*, Nature Communications **6**, 10167 (2015).
[50] S. Passlack, S. Mathias, O. Andreyev, D. Mittnacht, M. Aeschlimann, and M. Bauer, J. Appl. Phys. **100**, 024912 (2006).
[51] L. Bürgi, L. Petersen, H. Brune, and K. Kern, Surf. Sci. **447**, L157 (2000).
[52] A. A. Ünal, C. Tusche, S. Ouazi, S. Wedekind, C.-T. Chiang, A. Winkelmann, D. Sander, J. Henk, and J. Kirschner, Phys. Rev. B **84**, 073107 (2011).
[53] E. V. Chulkov, V. M. Silkin, and P. M. Echenique, Surf. Sci. **437**, 330 (1999).
[54] J. Kliewer, R. Berndt, E. V. Chulkov, V. M. Silkin, P. M. Echenique, and S. Crampin, Science **288**, 1399 (2000).
[55] M. Reutzel, A. Li, B. Gumhalter, and H. Petek, Phys. Rev. Lett. **123**, 017404 (2019).
[56] F. Haag, T. Eul, P. Thielen, N. Haag, B. Stadtmüller, and M. Aeschlimann, Review of Scientific Instruments **90**, 103104 (2019).
[57] E. Knoesel, A. Hotzel, and M. Wolf, J. Electron. Spectrosc. Relat. Phenom. **88-91**, 577 (1998).
[58] W. Berthold, U. Höfer, P. Feulner, E. V. Chulkov, V. M. Silkin, and P. M. Echenique, Phys. Rev. Lett. **88**, 056805 (2002).
[59] W. Berthold, J. Güdde, P. Feulner, and U. Höfer, Applied Physics B **73**, 865 (2001).
[60] A. Damm, K. Schubert, J. Güdde, and U. Höfer, Phys. Rev. B **80**, 205425 (2009).
[61] F. Himpsel and J. Ortega, Phys. Rev. B **46**, 9719 (1992).
[62] R. R. Freeman, P. H. Bucksbaum, H. Milchberg, S. Darack, D. Schumacher, and M. E. Geusic, Phys. Rev. Lett. **59**, 1092 (1987).
[63] M. Wollenhaupt, T. Bayer, and T. Baumert, in *Ultrafast Dynamics Driven by Intense Light Pulses: From Atoms to Solids, from Lasers to Intense X-rays*, edited by M. Kitzler, and S. Gräfe (Springer International Publishing, Cham, 2016), pp. 63.
[64] W. L. Schaich and N. W. Ashcroft, Solid State Commun. **8**, 1959 (1970).
[65] V. M. Silkin, P. Lazić, N. Došlić, H. Petek, and B. Gumhalter, Phys. Rev. B **92**, 155405 (2015).
[66] C. Timm and K. H. Bennemann, J. Phys.: Condens. Matter **16**, 661 (2004).
[67] T. Oka and S. Kitamura, Annual Review of Condensed Matter Physics **10**, 387 (2019).
[68] F. Mahmood, C.-K. Chan, Z. Alpichshev, D. Gardner, Y. Lee, P. A. Lee, and N. Gedik, Nat. Phys. **12**, 306 (2016).
[69] O. Reshef, I. De Leon, M. Z. Alam, and R. W. Boyd, Nature Reviews Materials **4**, 535 (2019).
[70] Y. Yang *et al.*, Nat. Phys. **15**, 1022 (2019).
[71] C. M. Li, L. E. Urbach, and H. L. Dai, Phys. Rev. B **49**, 2104 (1994).
[72] T. Rohwer *et al.*, Nature **471**, 490 (2011).
[73] I. Gierz *et al.*, Phys. Rev. Lett. **115**, 086803 (2015).

[74] C. W. Nicholson, A. Lücke, W. G. Schmidt, M. Puppin, L. Rettig, R. Ernstorfer, and M. Wolf, Science **362**, 821 (2018).